Characterization Study of CO$_2$, CH$_4$, and CO$_2$/CH$_4$ Hydroquinone Clathrates Formed by Gas−Solid Reaction

Romuald Coupan,[†] Eve Péré,[‡] Christophe Dicharry,[†⊙] Frédéric Plantier,[§] Joseph Diaz,[†] Abdel Khoukh,[‡] Joachim Allouche,[‡] Stephane Labat,[‡] Virginie Pellerin,[‡] Jean-Paul Grenet,[‡] Jean-Marc Sotiropoulos,[‡] Pascale Senechal,[∥] Fabrice Guerton,[∥] Peter Moonen,[†,∥] and Jean-Philippe Torré*,[†⊙]

[†]Laboratoire des Fluides Complexes et leurs Réservoirs IPRA, UMR5150, CNRS/Total/Université Pau and Pays Adour, Avenue de l'Université, 64000 Pau, France

[‡]Institut des Sciences Analytiques et de Physico Chimie pour l'Environnement et les Matériaux (IPREM), UMR 5254, Hélioparc, Université Pau and Pays Adour, Avenue du Président Pierre Angot, 64000 Pau, France

[§]Laboratoire des Fluides Complexes et leurs Réservoirs IPRA, UMR5150, CNRS/Total/Université Pau and Pays Adour, Allée du Parc Montaury, 64600 Anglet, France

[∥]Développement de Méthodologies EXpérimentales   IPRA, UMS 3360, CNRS/Université Pau and Pays Adour, Avenue de l'Université, 64000 Pau, France

● *Supporting Information*

ABSTRACT: Hydroquinone (HQ) is known to form organic clathrates with some gaseous species such as CO$_2$ and CH$_4$. This work presents spectroscopic data, surface and internal morphologies, gas storage capacities, guest release temperatures, and structural transition temperatures for HQ clathrates obtained from pure CO$_2$, pure CH$_4$, and an equimolar CO$_2$/CH$_4$ mixture. All analyses are performed on clathrates formed by direct gas−solid reaction after 1 month's reaction at ambient temperature conditions and under a pressure of 3.0 MPa. A collection of spectroscopic data (Raman, FT IR, and ^{13}C NMR) is presented, and the results confirm total conversion of the native HQ (α HQ) into HQ clathrates (β HQ) at the end of the reaction. Optical microscopy and SEM analyses reveal morphology changes after

the enclathration reaction, such as the presence of surface asperities. Gas porosimetry measurements show that HQ clathrates and native HQ are neither micro nor mesoporous materials. However, as highlighted by TEM analyses and X ray tomography, α and β HQ contain unsuspected macroscopic voids and channels, which create a macroporosity inside the crystals that decreases due to the enclathration reaction. TGA and in situ Raman spectroscopy give the guest release temperatures as well as the structural transition temperatures from β HQ to α HQ. The gas storage capacity of the clathrates is also quantified by means of different types of gravimetric analyses (mass balance and TGA). After having been formed under pressure, the characterized clathrates exhibit exceptional metastability: the gases remain in the clathrate structure at ambient conditions over time scales of more than 1 month. Consequently, HQ gas clathrates display very interesting properties for gas storage and sequestration applications.
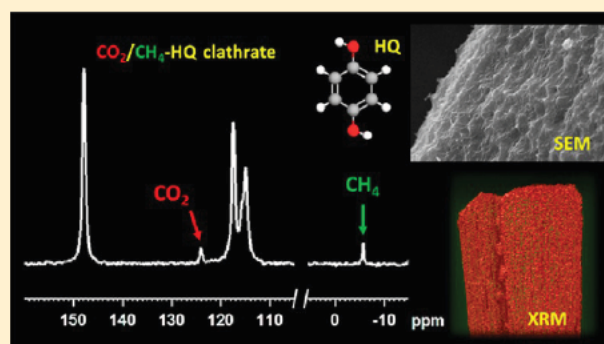
■ INTRODUCTION

Gas clathrates are inclusion compounds composed of a lattice of host molecules, capable of encaging low molecular weight gases as guest molecules.[1] The most studied clathrates are gas hydrates, where water acts as a host molecule.[2] It is also a well known fact that hydroquinone (1,4 dihydroxybenzene)—an organic compound of chemical formula C$_6$H$_4$(OH)$_2$ noted HQ in the following paper—forms organic gas clathrates.[3] This compound has four known polymorphisms: α, β, γ, and δ HQ, which require specific thermodynamic conditions to form.

α HQ is the stable form at ambient pressure and temperature conditions.[3] It belongs to the space group $R\overline{3}$ and has a rhombohedral lattice with parameters a = 38.5361 Å and c =

5.6641 Å.[4,5] A unit cell of α HQ is composed of 54 molecules and has a density of 1.33 g/cm^3.[1,5] The crystallographic arrangement of the molecules in this form of HQ creates cavities in the structure, which are able to accommodate small guest molecules such as CO$_2$, Ar, N$_2$, and H$_2$. The maximum host:guest ratio in α HQ—if each cavity contains one guest molecule—is 18:1 (i.e., 18 molecules of HQ per guest molecule).[5,6] The phenomenon of guest inclusion in the

cavities of the native HQ structure is called "solubilization in the α phase".

γ HQ is a metastable form prepared by sublimation (or rapid evaporation) of an HQ solution in ether.[3] The monoclinic lattice parameters of γ HQ, belonging to the space group $P2_1/c$, are $a = 8.07$ Å, $b = 5.20$ Å, $c = 13.20$ Å, and $\beta = 107°$. A unit cell is composed of 4 molecules of HQ and has a density of 1.380 g/cm^3. This form is not known to be an inclusion compound.[7,8]

δ HQ was observed only recently. This form has a slightly greater density than α HQ—approximately 1.37−1.40 g/cm^3—and was initially detected by exposing α HQ to high temperatures and pressures (greater than 440 K and 40 MPa).[9] Moreover, this "high pressure form" was also observed at ambient temperature by applying a mechanical pressure of about 5 GPa to N_2 and CH_4 HQ clathrates.[10,11] This structure corresponds to an amorphization of the host lattice induced by the release of the guest and is not an inclusion compound.

β HQ, the most versatile of all of the HQ structures, is the clathrate form which develops in the presence of guest molecules under well defined conditions of temperature and pressure.[3,12] Although the stability of clathrates generally depends on the presence of guest molecules inside the structure, a metastable guest free β HQ (i.e., a clathrate structure without any guest molecules inside) has been observed,[13−16] while the synthesis of such an empty clathrate is rather difficult.[16] The stoichiometry of the β HQ clathrate form is 3:1 (i.e., 3 molecules of HQ per guest molecule). Its chemical formula is $3C_6H_4(OH)_2 \cdot xG$, where G is the guest molecule in the clathrate structure and x is the clathrate occupancy (i.e., the proportion of cavities filled by guest molecules, ranging from 0 for guest free clathrates to 1 for full clathrates).[3,17−19] This stoichiometric relationship has been used to determine that the maximum storage capacity of HQ clathrates is 3.03 mol^{Guest}/kg^{HQ}. The highest clathrate occupancy observed so far is approximately 0.74 for the CO_2 HQ clathrates formed by crystallization from a solvent.[20−23] For CH_4 HQ, full occupancy has already been achieved (i.e., the clathrate occupancy is equal to 1).[23]

The HQ clathrates have an aerated structure generated by a hydrogen bonded organic framework. In β HQ, each HQ molecule contributes to the formation of two adjacent cavities owing to the two hydroxyl functions. The cavity results from the association of two groups of three HQ molecules.[24,25] The top and bottom of the clathrate cavity are formed by planar hexagonal rings $[OH]_6$ resulting from hydrogen bonding between the hydroxyl functions of six HQ molecules.[3] It was established there were three crystallographic types of β HQ: type I, II, or III depending on the nature, size, and shape of the encaged guest molecules.[3,24−26] β HQ clathrates of types I, II, and III belong to space groups $R3$, $R3$, and $P3$, respectively.[3,27] CO_2 HQ and CH_4 HQ clathrates are type I β HQ clathrates.[4,22,28] The rhombohedral lattice parameters for CH_4 HQ clathrates with an occupancy of 0.69 are $a = 16.44$ Å and $c = 5.65$ Å,[4,28] and those for CO_2 HQ clathrates with an occupancy of 0.74 are $a = 16.33$ Å and $c = 5.68$ Å.[13,28]

HQ clathrates can be synthesized in the liquid phase by recrystallization of dissolved HQ into guest molecules (such as CH_3CN and CH_3OH).[25,26] It is also possible to dissolve HQ in an appropriate solvent (such as n propanol, ethanol, or butyl acetate) and put this solution in contact with the guest. In this case, the solvent is not retained as a guest molecule because it is incompatible with the HQ clathrate cages. When the guest molecule is a gaseous species, the clathrates are prepared by pressurizing or bubbling the gas in a saturated HQ solution.[21,22,24] Other investigations have shown it is possible to form HQ clathrates in the solid phase by pressurizing powdered α HQ using guest molecules.[4,10,29,30] Using this method of synthesis it has been shown that HQ clathrates can represent an alternative for storing and transporting gases such as H_2,[15,31] CH_4,[10] and CO_2.[13] Moreover, the HQ clathrates formed in this way have recently been studied and evaluated as reactive media for separating binary gas mixtures such as CO_2/N_2,[32,33] CO_2/CH_4,[13] CO_2/H_2,[13,34] C_2H_6/C_2H_4,[35] and C_2H_4/CH_4.[36] Furthermore, the synthesis of clathrates by direct gas−solid reaction presents undeniable practical advantages, principally related to the absence of solvent: (i) there is no limitation on the quantity of HQ that can be used in the process unlike in the liquid phase synthesis method (where the solubility of the HQ in the solvent has to be considered); (ii) the synthesis can be carried out over a wide range of pressures and temperatures, which avoids the phase transitions (e.g., vaporization, crystallization) that occur when solvent is used; (iii) there are no restrictions as regards the diffusion of species through the solvent phase; (iv) in an industrial process (e.g., a gas separation unit), it is much easier to use a gas−solid reactor than a three phase one, where the issues of gas dispersion in the liquid phase and the handling of crystal slurry have to be considered inside the contactor. One of the main limitations of gas−solid synthesis should however be pointed out: the reaction kinetics. The solid−solid transition (i.e., from α to β HQ) is generally slower than crystallization from a solution. To this effect, we recently proposed innovative HQ based composite materials in which the formation of HQ clathrates can be strongly accelerated.[37] We are aware though that additional efforts are required to overcome these kinetic limitations so that these materials can be deployed on a large scale for industrial applications. Consequently, although the direct gas−solid enclathration reaction between HQ and gas appears to be a very promising solution for the storage, transportation, and selective capture of gases, the properties of HQ clathrates synthesized using this method need to be better understood.

For this study, CO_2, CH_4, and a CO_2/CH_4 mixture were chosen as the gases to react with the HQ. Indeed, the development of innovative and efficient processes for separating CO_2 from CO_2/CH_4 mixtures is of interest to the oil and gas, energy, and environmental sectors.[38] HQ clathrates were obtained by direct gas−solid reaction using HQ with pure CO_2, pure CH_4, and an equimolar CO_2/CH_4 mixture at ambient temperature and a pressure of 3.0 MPa. For example, these clathrate formation conditions could be a potential operating point for a natural gas sweetening unit (i.e., removal of CO_2 and H_2S). Although the spectroscopic signatures of various HQ clathrates have already been published in the literature, data sets based on samples obtained in identical synthesis conditions have not yet been presented in a cross complementary approach combining Raman, infrared (IR), and nuclear magnetic resonance (NMR) techniques. In addition, the surface and internal morphologies of clathrates resulting from a gas−solid reaction have not been sufficiently characterized to date, and the data on their gas storage capacities and thermal properties are very scarce or nonexistent in the literature. The purpose of this study is therefore to provide an extended set of characteristics concerning HQ clathrates obtained by gas−solid reaction. The clathrates were characterized using a wide range of experimental methods:

three spectroscopic techniques—Raman and Fourier transform IR (vibrational) and ^{13}C NMR—were used to obtain cross sectional data giving the key elements to easily identify the different structures and evaluate the reaction conversion from α to β HQ after the synthesis. Optical microscopy and scanning electron microscopy (SEM) analyses were performed to investigate the surface of the clathrates. For the first time transmission electron microscopy (TEM) analyses and X ray tomography were used to inspect the internal structure of the crystals. In addition, thermogravimetric measurements (TGA) coupled to mass spectrometry and in situ Raman spectroscopy were employed to identify the characteristic temperatures of the clathrates, such as the guest release temperatures and the structural transition temperatures from β HQ to α HQ. Finally, the gas storage capacity of the clathrates was quantified by means of gravimetric analyses and for the first time was studied for periods of more than 1 month.

■ EXPERIMENTAL SECTION

Materials. HQ (purity of 99.5 mol %) is provided by Acros Organics. In the experiments the native HQ (millimeter sized) is pure and unprocessed (e.g., not ground). The CO_2, CH_4, and CO_2/CH_4 mixture (minimum mole fraction purity of 99.995%) were purchased from Linde Gas SA. The CO_2 mole fraction of the CO_2/CH_4 mixture is 50.1 ± 1.0% (analytical value given by the supplier).

Apparatus and Procedures. *Synthesis of the HQ Clathrates.* The HQ clathrate samples were prepared using high pressure tank reactors, made of 316 stainless steel, connected to a pressurized gas storage tank and a vacuum pump that produces a primary vacuum of 0.0001 MPa throughout the system. The pressure during the experiment is controlled by a digital manometer (model LeoII from Keller with an uncertainty of ±0.01 MPa) located on top of the reactor. The masses of HQ introduced into the reactor are measured by means of an analytical balance (from Kern PLT) with an uncertainty of ±0.001 g. First, about 3.0 g of HQ was loaded into glass vessels plugged with cotton to avoid particle loss during the pressurization and depressurization steps. The vessels are then placed in the reactor. The air in the system is evacuated under vacuum and the reactors pressurized at 3.0 MPa with pure CO_2, CH_4, or CO_2/CH_4 for 1 month at ambient temperature. The pressure is kept constant throughout the experiment by continuously adding feed gas. Finally, the HQ clathrate samples are collected by depressurizing the system from 3.0 MPa to atmospheric pressure in a few minutes.

Analytical Methods for Characterizing HQ Clathrates. The clathrate samples are analyzed immediately after depressuriza tion of the reactor by spectroscopy (Raman, infrared, ^{13}C NMR), microscopy (optical, SEM, TEM), gas porosimetry, X ray tomography, and thermogravimetry. The characterization apparatuses and methods are described in the Supporting Information.

■ RESULTS AND DISCUSSION

Spectroscopic Identification. First, native α HQ and CO_2 HQ, CO_2/CH_4 HQ, and CH_4 HQ clathrate samples obtained after 1 month's reaction at 3.0 MPa and ambient temperature have been analyzed by Raman and IR spectrom etry (see Figures S1 and S2, Supporting Information). The spectroscopic data of theses clathrate crystals were found in very good agreement with literature data.[22,39−41] For the three

clathrates, the Raman bands corresponding to the HQ molecules are found at the same Raman shifts. In addition, the presence of CO_2 and CH_4 guest molecules is confirmed by specific Raman and IR bands, as also reported in the literature.[22,28,39,41,43,44] Interestingly, it is worth noting that the Raman and IR signatures of gas clathrates obtained in this work by direct/gas solid reaction and those obtained by crystallization from solvent[22] are similar.

The ^{13}C NMR spectra of the α HQ and CO_2 HQ, CO_2/CH_4 HQ, and CH_4 HQ clathrate samples are shown in Figure 1. Two groups of signals can be observed at around 118 and
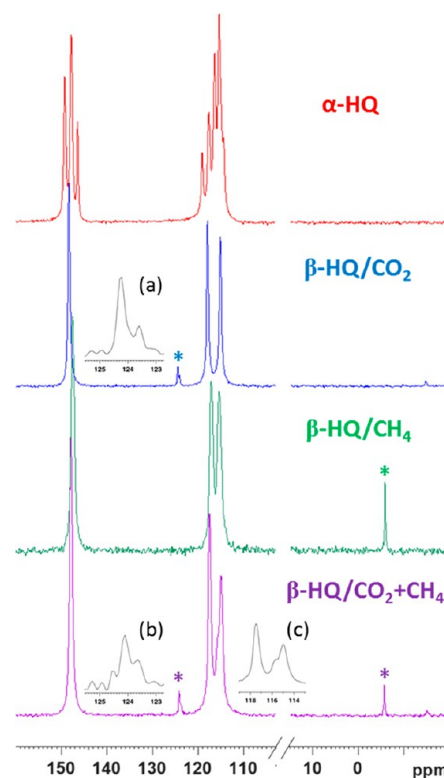

Figure 1. ^{13}C NMR spectra: (red) α HQ, (blue) β HQ/CO_2, (purple) β HQ/CO_2+CH_4, and (green) β HQ/CH_4 clathrates. Asterisks (*) show the signals observed for CO_2 and CH_4 molecules. Enlargements show the signals of the CO_2 guest molecules in the (a) CO_2 HQ and (b) CO_2/CH_4 HQ clathrates, and (c) signals of unsubstituted carbons in the CO_2/CH_4 HQ clathrates.

148 ppm for the α HQ sample. Integration of these groups of peaks gives a surface ratio of 4.0:2.3 (consistent with the theoretical ratio of 4:2 between unsubstituted and substituted carbons in HQ molecules). The first group of peaks at around 118 ppm therefore corresponds to unsubstituted carbon atoms, while the second one, at about 148 ppm, corresponds to hydroxyl substituted carbon atoms. The spectra of the clathrate samples exhibit three distinct peaks representing three inequivalent carbons. The peak with the highest chemical shift is attributed to hydroxyl substituted carbon atoms, and the two others correspond to unsubstituted carbon atoms. The HQ chemical shifts of the CO_2 HQ clathrates are observed at 147.9, 117.5, and 115.0 ppm and those of the CH_4 HQ clathrates at 147.8, 117.4, and 115.7 ppm. It is important to mention a noticeable difference in the chemical shifts of one of the unsubstituted carbon peaks (i.e., a difference of 0.7 ppm) that can be attributed to the different chemical environments of the

carbon atoms or to the HQ lattice distortions caused by the CO_2 molecules.[28] In the case of CO_2/CH_4 HQ clathrates, the HQ chemical shifts are observed at 147.9, 117.5, and 115.0 ppm. A shoulder can be seen at 115.7 ppm (see Figure 1c), which suggests that the carbon atoms from the HQ molecules have two different chemical environments. This double peak could be the result of heterogeneous host–guest interactions, specific to the CO_2 or CH_4 molecules. Another possibility is that different cavities coexist in these mixed HQ clathrates. By integrating these peaks, a surface ratio of around 80.5:19.5 is obtained for those at 115.0 and 115.7 ppm, respectively. The signal for CH_4 guest molecules is observed at −5.6 and −5.7 ppm in the case of CH_4 HQ and CO_2/CH_4 HQ clathrates, while the signal for CO_2 guest molecules is observed at 124.3 and 124.2 ppm in the case of CO_2 HQ and CO_2/CH_4 HQ clathrates. Interestingly enough, these two clathrates exhibit less pronounced shoulders, which means that the CO_2 molecules also have different chemical environments inside the clathrates. This might be due to specific interactions involving the guest molecules, as already observed and discussed in the literature.[22] The shoulder for the CO_2 HQ clathrates is detected at 123.6 ppm (see Figure 1a), yielding a surface ratio of 74.1:25.9 for the peaks at 124.3 and 123.6 ppm, respectively. However, in the case of the mixed CO_2/CH_4 HQ clathrates, the spectra exhibit two shoulders at 124.6 and 123.8 ppm (see Figure 1b) on either side of the main signal at 124.2 ppm. Integration of the peaks gives a surface ratio of 8.2:62.8:29.0 for the peaks at 124.6, 124.2, and 123.8 ppm, respectively. These three signals for CO_2 molecules suggest three possible environments resulting in the following interactions: (i) CO_2–CO_2, (ii) CO_2 empty cages, and (iii) CO_2–CH_4. It is worth noting that only one environment is detected for CH_4 molecules in the CH_4 HQ and CO_2/CH_4 HQ clathrates. This could mean that the interactions involving CH_4 molecules might be below the detectability limit of our NMR spectrometer. By integrating the peaks of the CO_2 and CH_4 guest molecules, an average ratio of 1.6 ± 0.2 mol^{CO2}:mol^{CH4} was estimated for the CO_2/CH_4 mixture retained in the clathrate, indicating a slight trend for preferential capture of CO_2 molecules in the initial equimolar CO_2/CH_4 mixture.

Finally, after 1 month of gas–solid reaction, all spectroscopic analyses performed confirmed that all samples had been totally converted from α HQ to gas clathrates.

Crystal Morphology and Topography. Surface observations were performed by optical microscopy and SEM. Figure 2 shows optical microscopy images of α HQ and CO_2 HQ, CO_2/CH_4 HQ, and CH_4 HQ clathrate samples which present visual evidence that changes occur after the enclathration reaction. α HQ has a shiny surface, whereas the clathrates appear dull and whitish to the naked eye.

SEM images of the samples are shown in Figure 3. The native α HQ crystal (Figure 3a and 3b) has a flat, smooth surface, while all HQ clathrates (Figure 3c–h) have a rough aspect. Differences in texture can also be seen between the CO_2 HQ and the CH_4 HQ clathrates (Figure 3c and 3d and 3e and 3f): the surface of the CH_4 HQ clathrates exhibits different sized nodules, while the surface of the CO_2 HQ clathrates presents regular and ordered asperities. The surface of the CO_2/CH_4 HQ clathrates combines features of both the CO_2 HQ and the CH_4 HQ clathrate surfaces (Figure 3g and 3h). In addition, for both clathrate samples, multiple macro pores (which look like perforations, as shown in Figure 3f and 3h) from 500 nm to 1 μm were detected.
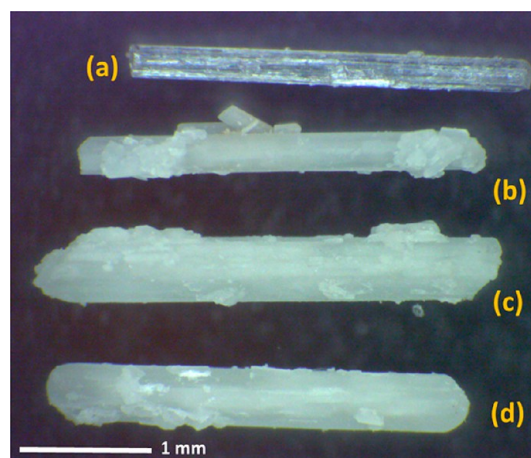

Figure 2. Optical microscopy images of (a) α HQ and (b) CO_2 HQ, (c) CO_2/CH_4 HQ, and (d) CH_4 HQ clathrates.

The inside of the clathrate crystals was examined by TEM and X ray tomography. Figure 4 shows TEM images of the α HQ and CO_2 HQ, CO_2/CH_4 HQ, and CH_4 HQ clathrate samples. The structure of the clathrates is macroporous with large, relatively compact cavities of approximately 80−100 nm. This result corroborates those of gas porosimetry experiments, which revealed negligible quantities of gas adsorbed on both the HQ clathrates and the native HQ, suggesting the absence of micro and mesoporosity (i.e., pores smaller than 50 nm in diameter). The latter observation is in agreement with the literature.[13] In addition, the structure of the CO_2 HQ clathrates (Figure 4c and 4d) appears to have suffered more damage during the enclathration process than that of the CO_2/CH_4 HQ and CH_4 HQ clathrates.

For the very first time X ray tomography was used on HQ to obtain more details on its internal structure and the morphological changes induced by the enclathration reaction. Six crystals of α HQ were attached to independent metallic needles in an attempt to image both their native state (α HQ) and their state after reaction with CO_2 (β HQ) as described earlier, namely, exposure for 1 month at ambient temperature and a pressure of 3 MPa. We were able to fully analyze two out of six crystals (i.e., perform initial scanning, pressurization, reaction, depressurization, final scanning, as well as all intermediate handling). Their initial morphologies were different, yet all reaction induced phenomena were quantitatively comparable, suggesting that the phenomena observed are representative. For clarity, only the results of one sample are discussed in detail.

Figure 5 presents a qualitative comparison of the crystal characteristics observed before and after the reaction. Differences in surface texture before (Figure 5a) and after (Figure 5d) enclathration can be observed. The α HQ surface is flat and has a number of longitudinal striations before the reaction (in green), while it is very rough afterwards. This alteration of the surface texture can also be seen on a zoomed in image of a longitudinal cross section through the crystal (see Figure 5c and 5f). The roughening of the crystal surface after the reaction is consistent with the SEM observations (see Figure 3). On the basis of the X ray data it is also possible to analyze the inside of the crystal. A small number of large voids ranging from 1 μm to a few tens of micrometers in size can be seen in the crystal (Figure 5b and 5e) that appears otherwise to be totally homogeneous. The size—and to some extent the shape—of
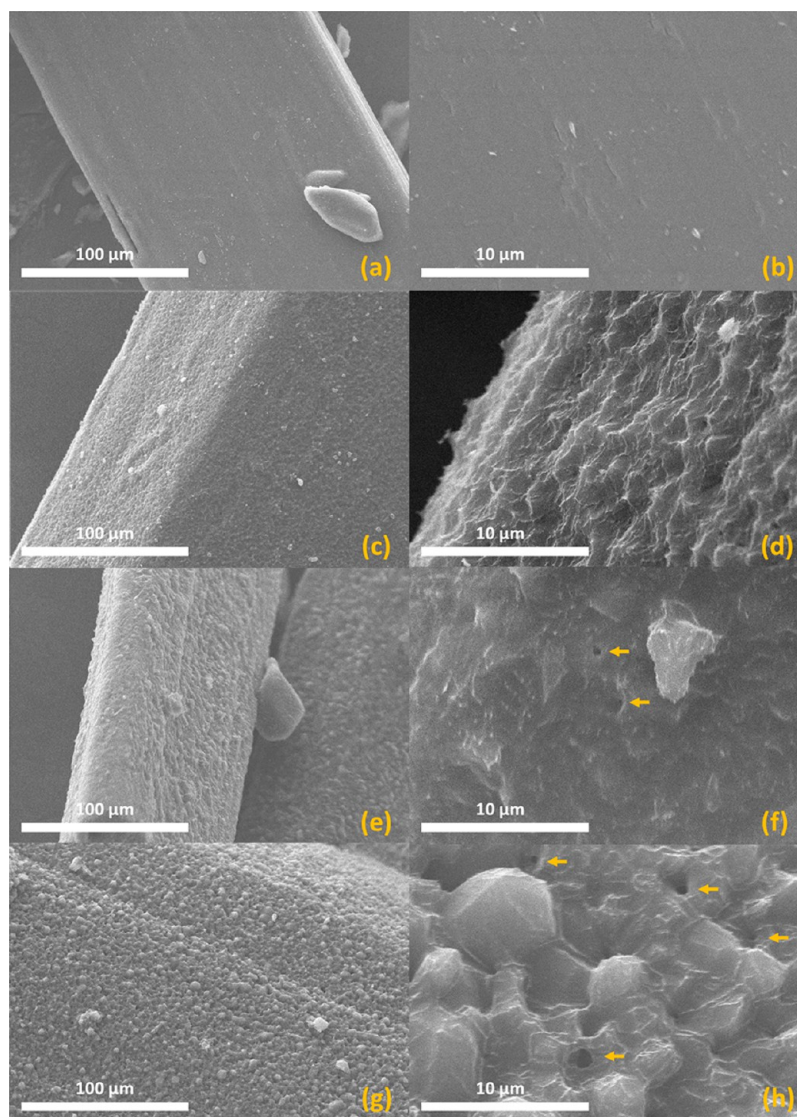
Figure 3. SEM images. (a, b) α HQ, (c, d) CO_2 HQ, (e, f) CH_4 HQ, and (g, h) CO_2/CH_4 HQ clathrates. Arrows indicate macropores.

these voids appears to be altered when the surrounding crystal lattice transforms from α into β HQ.

A quantitative analysis of key morphological parameters derived from the X ray data is presented in Figure 6. These parameters are plotted as a function of the longitudinal position in the crystal for both the α HQ and the CO_2 HQ clathrates. The uncertainty bands conservatively account for the major errors in the image analysis process.

First, the volume of the crystal matrix (Figure 6a) and the visible pores (Figure 6b) were analyzed. As can be observed, the volumes of both the matrix and the pores change after the enclathration reaction. The crystal cross sections reveal a loss in matrix volume along the outer crystal surface and an increase in matrix volume around the large pores, inducing a reduction in pore volume. This would suggest a crystal which expands uniformly due to the transformation from α HQ to β HQ and whose outer surface is subsequently eroded. This hypothesis also explains why the reduction in pore volume is fairly uniform along the entire length of the investigated portion of the crystal, while the change in matrix volume is not at all uniform and is prone to uncertainty. Indeed, as the latter is the result of two

opposing processes (expansion and erosion), its net result depends on the competition between both processes.

Next, the visible porosity (i.e., the visible pore volume divided by the matrix volume) was analyzed (Figure 6c and 6d). Note that gas porosimetry (see above) demonstrated the absence of micro and mesopores, implying that the visible porosity should be close to the actual porosity. The visible porosity exhibits a fairly constant reduction over the entire length of the crystal. This reduction amounts to 0.5% or one half of the visible pore volume and is related to the expansion of the HQ lattice when α HQ transforms into β HQ.[1]

X ray tomography results also revealed the presence of fractures inside one of the CO_2 HQ clathrates being analyzed. These fractures were not present in the native clathrates. Figure 7 shows a typical fracture. Although it is not possible to elucidate the origin of the fracturing process based on these observations, they are however consistent with a fracture formed during the depressurization step. As the crystal transforms from α HQ to β HQ it expands and internal stresses develop. When the reactor is depressurized (from 3 MPa to ambient pressure), the pressure reduction is not uniform: the pressure on the outer crystal surface equilibrates
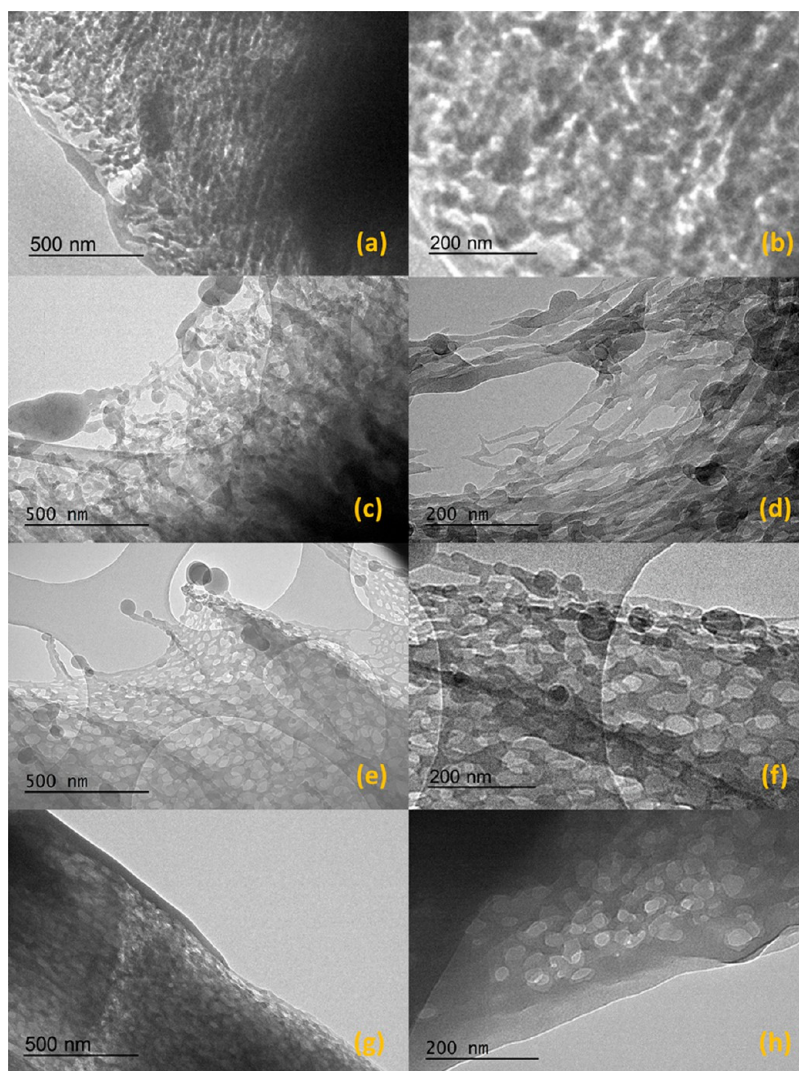
Figure 4. TEM images of (a, b) α HQ, (c, d) CO_2 HQ, (e, f) CO_2/CH_4 HQ, and (g, h) CH_4 HQ clathrates.
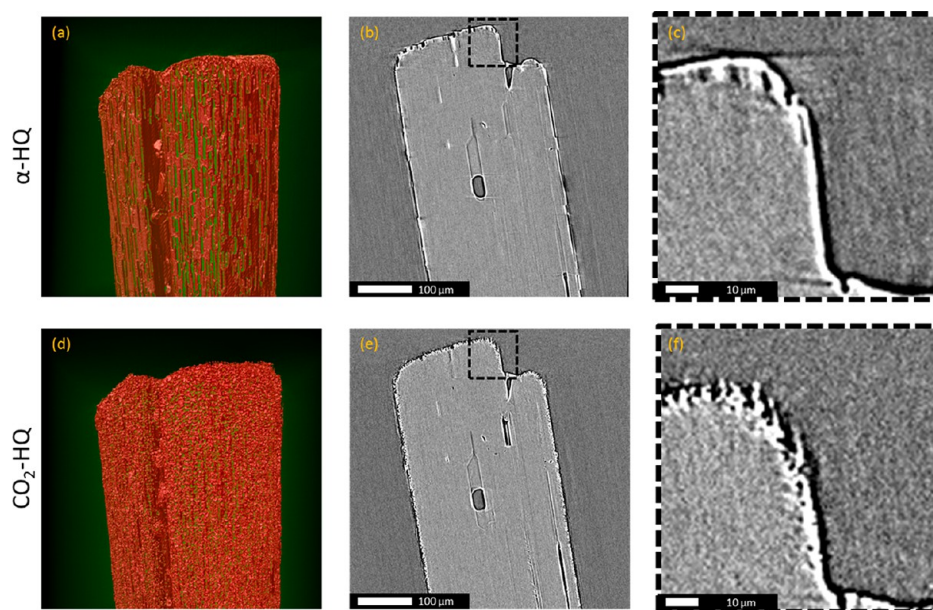

Figure 5. X ray tomography images of a single α HQ crystal (top) and of the same crystal after enclathration with CO_2 (bottom): (a, d) 3D view in false color of the top of the crystal, (b, e) longitudinal cross section, and (c, f) zoom on a region of interest of b and e.
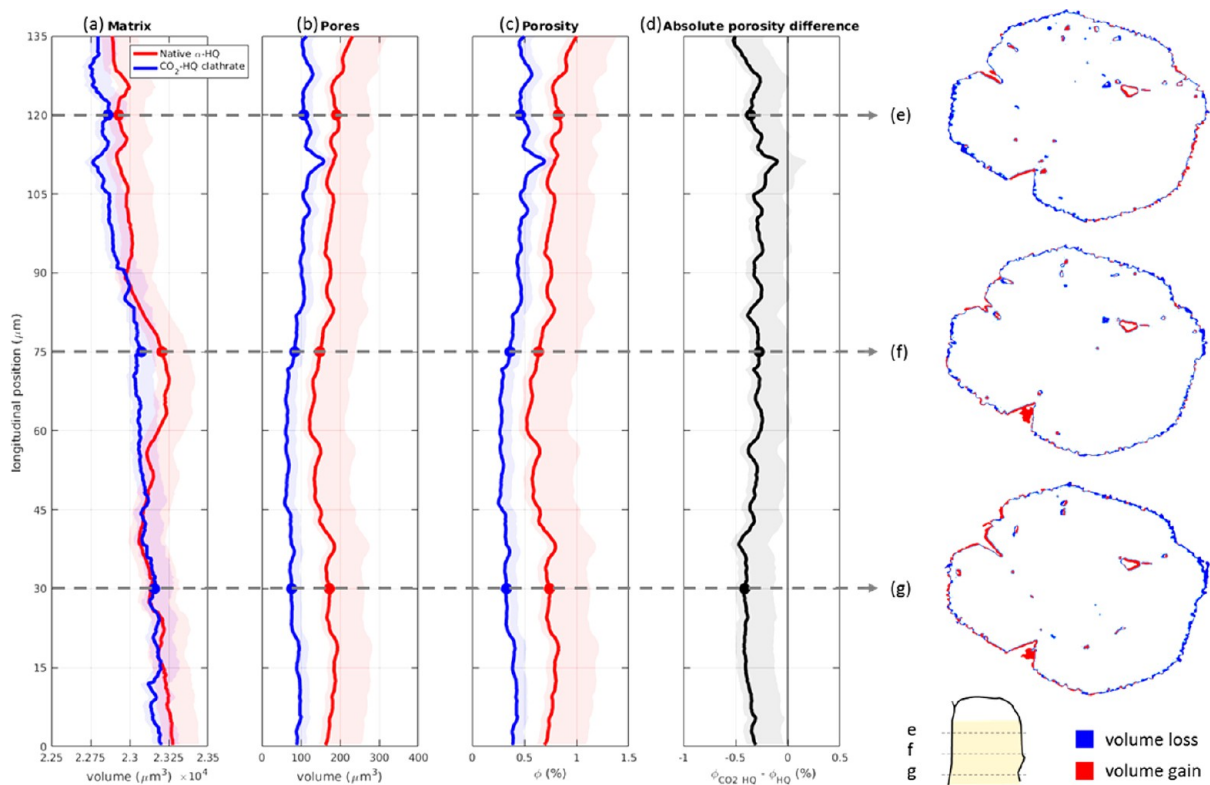
Figure 6. Key morphological parameters of α HQ and CO_2 HQ clathrates as a function of the vertical position in the crystal: volume of (a) matrix and (b) pores, (c) porosity, and (d) difference in porosity induced by the reaction. Shaded bands correspond to the estimated uncertainty on the parameters obtained. (e−g) Cross section through the crystal at three different heights illustrating the spatial location of the reaction induced volume changes.
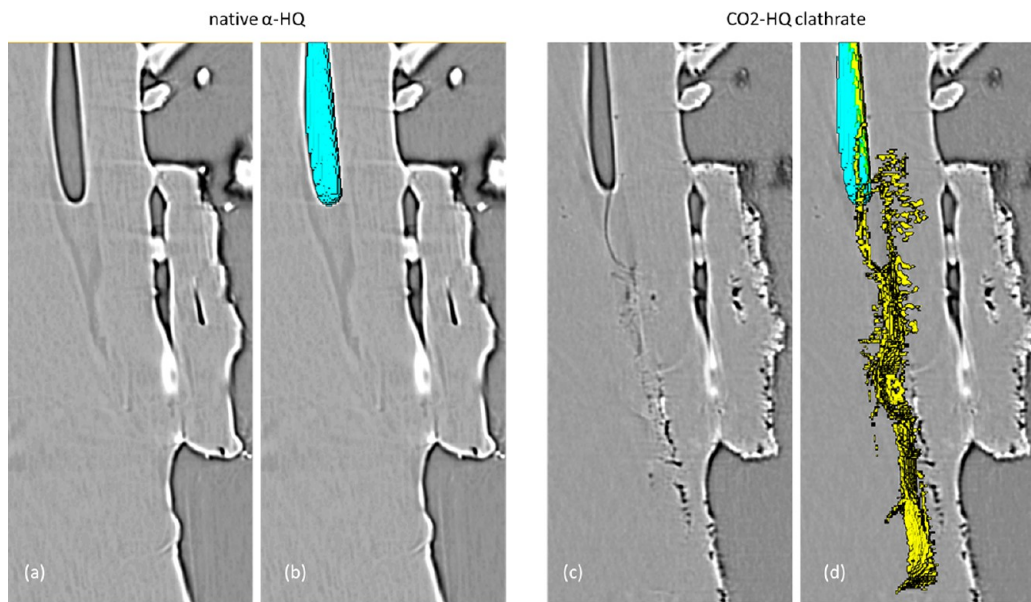

Figure 7. X ray tomography cross sections (2D images) of the second crystal analyzed (a, b) before and (c, d) after enclathration. (b and d) 3D pore volume (in blue) and 3D fracture (in yellow).

almost instantaneously, while the pressure reduction rate inside the pores is limited by the connectivity of the pores to the reactor volume. If the temporary overpressure that exists inside poorly connected pores and the internal stresses induced by the lattice transformation locally exceed the crystal's resistance, a fracture is initiated. If this hypothesis holds true, the "fragility" of clathrates that has often been observed could be overcome by modifying the pressure release rates. Further research should either support or falsify this hypothesis.

Physical Properties, Gas Storage Capacity, and Kinetic Stability. This section investigates some physical properties such as the gas release and structural transition temperatures (from β HQ to α HQ) as well as the gas storage capacities of the clathrates obtained by gas−solid reaction and their
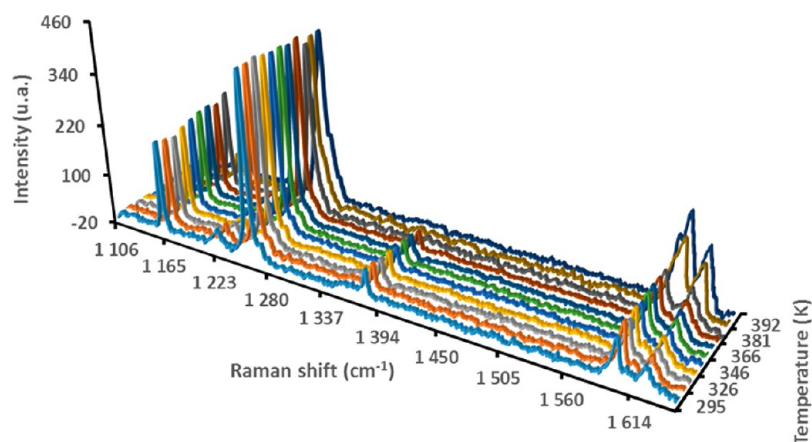
Figure 8. Structural tracking of the CO_2 HQ clathrates by Raman spectroscopy as a function of temperature.

metastability (i.e., the capacity of the clathrate structure to exist outside of its thermodynamic stability domain).

In situ Raman spectroscopy experiments were performed at atmospheric pressure. Figure 8 shows an example of the structural tracking of the CO_2 HQ clathrates by Raman spectroscopy as a function of temperature.

For both clathrates we can see a slight decrease in the guest band intensities for temperatures of up to about 360 K. The band intensities of the guests then significantly decrease from 360 K to the structural transition temperature when the structure reverses from β HQ to α HQ, and no more gas is retained in the structure. The structural transition for CO_2 HQ, CO_2/CH_4 HQ, and CH_4 HQ clathrates can be observed at 381 ± 5, 383 ± 6, and 378 ± 5 K, respectively. Although the magnitude of the temperature uncertainties varies significantly, our experimental $\beta \rightarrow \alpha$ transition temperatures were found to be in good agreement with values reported by Park et al.[42] Similar experiments performed under primary vacuum revealed that the structural transition temperatures are little affected by gas pressure. Indeed, for CO_2 HQ, CO_2/CH_4 HQ, and CH_4 HQ clathrates, the transitions occurred at 379 ± 5, 381 ± 6, and 378 ± 6 K, respectively. Up to a temperature of 393 K and a pressure of 1.0 MPa, neither structural transition nor significant gas releases induced by the corresponding guest molecules were detected, demonstrating for the first time that these clathrates are apparently stable under these conditions of pressure and temperature.

In the specific case of CO_2 HQ clathrates, a stunning and undocumented phenomenon was observed under specific temperature conditions. Indeed, when CO_2 HQ clathrates—collected for a few minutes to up to 48 h after opening of the reactor—are exposed to a temperature increase, they start "hopping" when the temperature exceeds about 350−363 K. This phenomenon is followed by rapid fragmentation and scattering of shards of crystal. For example, if the crystal is placed on a Kofler bench and moved slowly from the low to the high temperature zone, the crystal can be seen "jumping" over several tens of centimeters. Additionally, if the crystals are placed in a Raman cell and heated, they "hit" the sapphire windows located 10 mm above. Finally, in an attempt to monitor the evolution of clathrate crystal morphology after dissociation, we placed the crystals (those mounted on needles which were imaged by tomography after reaction) in a stove at 70 °C for 8 h immediately after X ray analysis; none of the crystals survived this step as they all were reduced to fragments

scattered inside the stove. In light of the many observations we made we called this phenomenon "the popcorn effect" as the "hopping" of these crystals when they are heated is similar to the popping of a grain of corn when heated. We noticed that this effect occurred at atmospheric pressure but also under primary vacuum. Interestingly enough, it was not observed for the CO_2/CH_4 HQ and CH_4 HQ clathrates. The origin of this phenomenon appears to be related to the specific enclathration of CO_2 as a guest molecule. As suggested in the literature, thermal stability is greatly affected in the case of HQ clathrates with distorted cavities (such as CO_2 HQ clathrates).[20] In this case, it appears that the significant degree of movement of the CO_2 molecules within the distorted clathrate cavities increases with temperature and could potentially damage the HQ host lattice. Investigations are in progress in our laboratory to gain greater understanding of the phenomenon.

The release of the gas molecules from the clathrate structure and the enclathration capacity were studied by TGA coupled with mass spectrometry. The TGA profiles obtained with the three clathrates (i.e., the evolution of the sample mass versus temperature) are shown in Figure 9. The nature of the gas
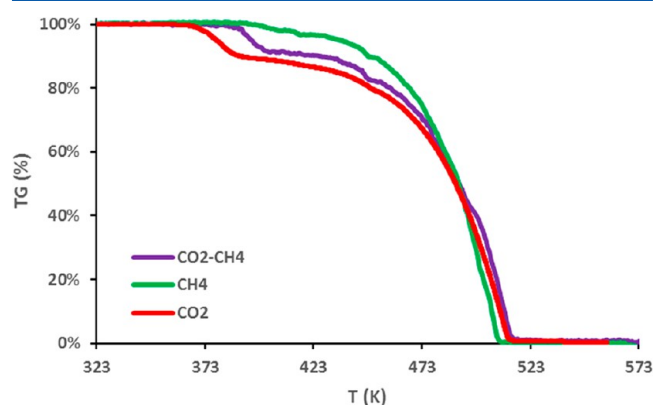
Figure 9. TGA curves of (purple) CO_2/CH_4 HQ, (green) CH_4 HQ, and (red) CO_2 HQ clathrates.

released during the clathrate dissociation was confirmed by mass spectrometry analysis, where the fragment ions of CO_2 (44, 28, 16, and 12) and CH_4 (16, 15, 14, 13, and 12) were detected. The thermograms clearly show two characteristic mass losses corresponding to first (i) the guest release and then (ii) the HQ sublimation/vaporization. Accordingly, the

calculation of the clathrate occupancy was performed without any correction concerning the volatility of HQ.

On the basis of the TGA curves we can see that the gas molecules enclosed in CO_2 HQ, CO_2/CH_4 HQ, and CH_4 HQ clathrates start being released from about 363 ± 2, 383 ± 2, and 390 ± 2 K, respectively. The data obtained are in good agreement with the average dissociation temperatures of 376.5 and 402.6 K reported by McAdie for CO_2 HQ and CH_4 HQ clathrates, respectively.[20] The gas release temperature for the mixed CO_2/CH_4 HQ clathrates is between the ones for CH_4 HQ and CO_2 HQ clathrates, which shows that the guest molecules logically depend upon the release temperature. This difference in gas release temperatures for the CO_2 HQ, CO_2/CH_4 HQ, and CH_4 HQ clathrates confirms (i) the greater thermal stability of CH_4 HQ clathrates and (ii) the role played by CH_4 molecules in the thermal stabilization of the mixed CO_2/CH_4 HQ clathrates, as already pointed out in the literature.[42]

In the case of CO_2/CH_4 HQ and CH_4 HQ clathrates, the start of release temperatures were, respectively, equal to and higher than their measured structural transition temperatures (i.e., 383 ± 6 K for CO_2/CH_4 HQ and 378 ± 5 K for CH_4 HQ clathrates) above which no more gas is theoretically retained in the structure. Indeed, by applying a heating rate of 5 K/min during the TGA, the HQ clathrates dissociate at a higher temperature than at the rate of 1 K/min set for the in situ Raman experiments. The dependency of the start of release temperatures on the heating rate shows that the system does not have enough time to reach equilibrium at high heating rates. Furthermore, the clathrate samples were analyzed beyond their stability range, and it came as no surprise that the heating rate affects the clathrate dissociation kinetics. Finally, it is important to note that both the structural transition temperature and the release temperature do not characterize thermodynamic transitions but point at which phenomena are kinetically noticeable.[20]

Using two independent techniques (TGA measurements and mass balance), the gas storage capacities of the HQ clathrates were calculated, and the results obtained are listed in Table S1. The clathrate occupancies calculated from the gas storage capacities are presented graphically in Figure 10. It is worth noting that the results obtained from mass balance and TGA are in excellent agreement, confirming the reliability of the data obtained.

First, for the same thermodynamic conditions and reaction time, the gas storage capacity of the CO_2 HQ clathrates was found to be relatively high, corresponding to an averaged clathrate occupancy of 0.94 ± 0.05 (close to unity). This value is consistent with literature data obtained from gas−solid reactions carried out in comparable experimental conditions: about 0.91−1.0 was found for 7 days' reaction between powdered HQ and CO_2 at 298 K and 3.0 MPa[33] and 0.95 for the reaction between powdered HQ and a CO_2/H_2 mixture in which the CO_2 had a partial fugacity of at least 1.8 MPa at 298 K.[34] Note that other authors have found lower clathrate occupancy values in different experimental conditions: 0.74 was obtained for 30 h of gas−solid reaction at 293−353 K and at a CO_2 pressure of 4.0 MPa[13] and 0.76 after 45 days of reaction at 323 K and 3.0 MPa.[37] Furthermore, our occupancy result is also higher than what is generally found for CO_2 HQ clathrates formed by crystallization from a solvent.[20−23] This point is not surprising as the method for synthesizing gas−solid clathrates is different from the one used for "liquid phase" synthesis.
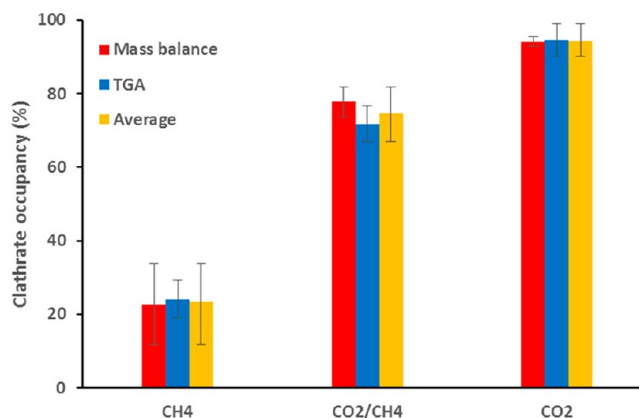

Figure 10. Clathrate occupancy for CH_4 HQ, CO_2/CH_4 HQ, and CO_2 HQ clathrates obtained after 1 month's reaction at 3.0 MPa and at ambient temperature. Results of (red) mass balance and (blue) TGA, and (yellow) average of mass balance and TGA values.

Consequently, we can assume that it is possible to reach occupancies very close to unity (such as those found in our study with $x = 0.94 \pm 0.05$) when the gas−solid reaction is performed in suitable operating conditions.

Second, in contrast to the very high occupancy value obtained with pure CO_2, it is obvious that the CH_4 HQ clathrates contain much less gas than the others, as their gas storage capacity was found to be around 4 times lower than that of the CO_2 HQ clathrates for example (see Table S1). Lower occupancy values for CH_4 HQ clathrates were also found at equilibrium conditions by Coupan et al.[45] Interestingly enough, the gas storage capacity of the CO_2/CH_4 HQ clathrates (i.e., 2.26 ± 0.24 mol/kg^{HQ}) was found to be midway between those of CO_2 HQ and CH_4 HQ clathrates.

Finally, in order to check the stability of the clathrates synthesized by gas−solid reaction, CO_2 HQ and CO_2/CH_4 HQ clathrates were exposed to ambient conditions over a long period (52 and 35 days for the CO_2 HQ and CO_2/CH_4 HQ clathrates, respectively) and the remaining gas was quantified versus time. The evolution of the storage capacity (evaluated by mass balance) over time is plotted in Figure 11. We did not perform this investigation for the CH_4 HQ clathrates as their occupancy was already very low after the synthesis.

The storage capacities of the CO_2 HQ clathrates decreased to 2.06 mol^{CO2}/kg^{HQ} ($x = 0.68$). Moreover, two successive release steps were observed: (i) a "fast" CO_2 release phase for the first 5 days followed by (ii) a slow CO_2 release phase for the
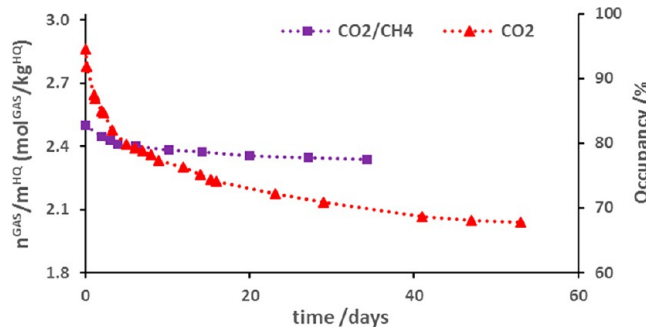

Figure 11. Gas storage capacities of (red) CO_2 HQ and (purple) CO_2/CH_4 HQ clathrates exposed to ambient conditions as a function of time.

rest of experiment. On the basis of our data we were able to estimate two release rates (from linear regression), namely, 82.3 and 7.4 $mmol^{CO2}/kg^{HQ}/day$ (decrease of 2.7% and 0.2% per day of the clathrate occupancy). The second gas release phase was of the same order of magnitude as the one found for CO_2 HQ clathrate monocrystals obtained by crystallization from a solvent (i.e., constant release rate of 29.5 $mmol^{CO2}/kg^{HQ}/day$, corresponding to a decrease in clathrate occupancy of 1.0% per day).[22]

The storage capacities of the CO_2/CH_4 HQ clathrates decreased from 2.50 to 2.33 mol^{CO2}/kg^{HQ} ($x = 0.77$) after 35 days. We also observed two successive release steps of 16.1 and 2.3 $mmol^{CO2}/kg^{HQ}/day$ (decrease in the clathrate occupancy of 0.5% and 0.1% per day). According to our measurements, we believe that the fast gas release phase is more noticeable in the case of HQ clathrates containing a large amount of gas. It is probable that the threshold capacity for which only the slow release phase can be seen lies between the capacity of the CO_2/CH_4 HQ clathrates (2.26 ± 0.24 mol^{CO2}/kg^{HQ} ($x = 0.75 \pm 0.07$)) and that of monocrystals (2.15 mol^{CO2}/kg^{HQ} ($x = 0.71$), as reported in the literature).[22] Moreover, it clearly appears that the gas release kinetics were slower for the mixed HQ clathrates than for the CO_2 HQ clathrates. The presence of CH_4 molecules inside the structure could have well impeded the diffusion of the molecules through the connected clathrate cavities. It would therefore be very interesting to perform complementary experiments (e.g., by neutron diffraction) to study the gas diffusion processes inside this clathrate structure.

It was the very first time that (i) clathrate metastability was investigated over such long period of time and (ii) that this type of two phase gas release kinetics was reported in the literature. In light of these results, we can say that the CO_2 HQ and CO_2/CH_4 HQ clathrates present remarkable structural metastability at ambient conditions, i.e., outside of their range of thermodynamic stability.[45] This property opens up interesting avenues for developing innovative gas storage and sequestration materials, particularly for CO_2 in ambient storage conditions.

CONCLUSIONS

HQ clathrates were obtained from pure CO_2, pure CH_4, and an equimolar CO_2/CH_4 mixture by direct gas–solid reaction after 1 month in high pressure reactors at ambient temperature and at 3.0 MPa. Cross spectroscopic analyses performed on samples obtained in the same reaction conditions were presented and discussed. Interestingly enough, ^{13}C NMR analyses revealed multiple peaks for the guest molecules located inside the cavities, leading us to conclude that complex interactions take place between them and suggesting that different cavities might coexist inside the clathrate structure, particularly in the case of the CO_2/CH_4 mixed HQ clathrates. In addition, the ^{13}C NMR signature of the clathrates obtained by reaction of the gas mixture with the α HQ revealed that the amount of CO_2 enclathrated in the structure is higher than the amount of CH_4 with a molar ratio of around 1.6 ± 0.2 mol^{CO2}/mol^{CH4}. The morphology and internal structure of the clathrate samples, investigated by microscopy (optical, SEM, TEM) and X ray tomography, gave us visual evidence that the enclathration process effectively occurred. Indeed, to the naked eye, the clathrates had a dull whitish aspect and exhibited surface asperities, whereas the α HQ had a smooth shiny surface. Moreover, TEM and X ray tomography highlighted that the clathrates contained macropores of up to several tens of micrometers in size. This macroporosity was shown to decrease when the HQ transformed from its native α form into CO_2 HQ clathrates: the volume of the HQ host lattice expanded. The gas storage capacities and characteristic temperatures of the clathrates obtained were investigated. For the CO_2 HQ, CO_2/CH_4 HQ, and CH_4 HQ clathrates, gas release started from around 363, 383, and 390 K when a heating rate of 5 K/min was applied, while the structural transitions from β to α HQ were observed at 379 ± 5, 381 ± 6, and 378 ± 6 K, respectively, at a rate of 1 K/min. The gas storage capacity of the CO_2 HQ clathrates, of approximately 2.85 ± 0.16 mol^{CO2}/kg^{HQ}, was greater than that of the CO_2/CH_4 HQ and CH_4 HQ clathrates. This capacity corresponds to a clathrate occupancy of 0.94 ± 0.05. Furthermore, we highlighted a phenomenon specific to CO_2 HQ clathrates called the popcorn effect, corresponding to the crystals hopping and fragmenting at around 350−363 K. Finally, the CO_2 and CO_2/CH_4 clathrates exhibited a progressive gas release at ambient conditions depending on the guest enclosed (faster for CO_2 than for the CO_2/CH_4 mixture) without any structural reversion over an extended period of more than 1 month. This last observation highlighted a very interesting property of HQ clathrates which could be used in future applications as inclusion compounds for gas storage and sequestration. However, we demonstrated that the CO_2 enclathration reaction created cracks in the native HQ crystals, making them more fragile. The fact both that native or powdered crystals develop small gas−solid surface areas and that CO_2 HQ clathrate crystals break very easily implies that HQ will have to be conditioned in a more robust material than crystals for it to be of use on a large scale for practical applications.

ASSOCIATED CONTENT

● Supporting Information

The Supporting Information is available free of charge on the ACS Publications website at DOI: 10.1021/acs.jpcc.7b07378.

Characterization apparatuses and methods; Raman and IR of HQ clathrates; gas storage capacities of HQ clathrates (PDF)

AUTHOR INFORMATION

Corresponding Author
*Phone: +33 (0)5 40 17 51 09. E mail: jean philippe.torre@univ pau.fr.

ORCID ●
Christophe Dicharry: 0000 0002 6318 3989
Jean-Philippe Torré: 0000 0001 5735 8626

Author Contributions
All authors contributed extensively to the work presented in this paper and have approved the final version.

Notes
The authors declare no competing financial interest.

Versa 510T used to carry out the tomographic acquisitions reported in this article.

■ REFERENCES

(1) Powell, H. M. The Structure of Molecular Compounds. Part IV. Clathrate compounds. *J. Chem. Soc.* **1948**, 61−73.

(2) Sloan, E. D. Gas hydrates: Review of Physical/Chemical Properties. *Energy Fuels* **1998**, *12*, 191−196.

(3) Mak, T. C. W.; Lam, C. K. In *Encyclopedia of Supramolecular Chemistry*; Atwood, J. L., Steed, J. W., Eds.; CRC Press, Taylor & Francis Group: Boca Raton, FL, 2004; Vol. *1*, pp 679 − 686.

(4) Lee, J. W.; Lee, Y.; Takeya, S.; Kawamura, T.; Yamamoto, Y.; Lee, Y. J.; Yoon, J. H. Gas Phase Synthesis and Characterization of CH_4 Loaded Hydroquinone Clathrates. *J. Phys. Chem. B* **2010**, *114*, 3254−3258.

(5) Wallwork, S. C.; Powell, H. M. The Crystal Structure of the α Form of Quinol. *J. Chem. Soc., Perkin Trans. 2* **1980**, *2*, 641−646.

(6) Yoon, J. H.; Lee, Y. J.; Park, J.; Kawamura, T.; Yamamoto, Y.; Komai, T.; Takeya, S.; Han, S. S.; Lee, J. W.; Lee, Y. J. Hydrogen Molecules Trapped in Interstitial Host Channels of α Hydroquinone. *ChemPhysChem* **2009**, *10*, 352−355.

(7) Maartmann Moe, K. The Crystal Structure of γ Hydroquinone. *Acta Crystallogr.* **1966**, *21*, 979−982.

(8) Caspari, W. A. The Crystal Structure of Quinol. Part II. *J. Chem. Soc.* **1927**, *0*, 1093−1095.

(9) Naoki, M.; Yoshizawa, T.; Fukushima, N.; Ogiso, M.; Yoshino, M. A New Phase of Hydroquinone and its Thermodynamic Properties. *J. Phys. Chem. B* **1999**, *103*, 6309−6313.

(10) Lee, Y.; Lee, J. W.; Lee, H. H.; Lee, D. R.; Kao, C. C.; Kawamura, T.; Yamamoto, Y.; Yoon, J. H. High Pressure Investigation of α Form and CH_4 loaded β Form of Hydroquinone Compounds. *J. Chem. Phys.* **2009**, *130*, 124511.

(11) Kim, B. S.; Lee, Y.; Yoon, J. H. Pressure Dependent Release of Guest Molecules and Structural Transitions in Hydroquinone Clathrate. *J. Phys. Chem. B* **2013**, *117*, 7621−7625.

(12) Eikeland, E.; Thomsen, M. K.; Madsen, S. R.; Overgaard, J.; Spackman, M. A.; Iversen, B. B. Structural Collapse of the Hydroquinone Formic Acid Clathrate: A Pressure Medium Depend ent Phase Transition. *Chem. Eur. J.* **2016**, *22*, 4061−4069.

(13) Lee, Y. J.; Han, K. W.; Jang, J. S.; Jeon, T. I.; Park, J.; Kawamura, T.; Yamamoto, Y.; Sugahara, T.; Vogt, T.; Lee, J. W.; et al. Selective CO_2 Trapping in Guest Free Hydroquinone Clathrate Prepared by Gas Phase Synthesis. *ChemPhysChem* **2011**, *12*, 1056−1059.

(14) Evans, D. F.; Richards, R. E. Preparation and Magnetic Susceptibility of an Oxygen Clathrate Compound. *Nature* **1952**, *170*, 246.

(15) Han, K. W.; Lee, Y. J.; Jang, J. S.; Jeon, T. I.; Park, J.; Kawamura, T.; Yamamoto, Y.; Sugahara, T.; Vogt, T.; Lee, J. W.; et al. Fast and Reversible Hydrogen Storage in Channel Cages of Hydroquinone Clathrate. *Chem. Phys. Lett.* **2012**, *546*, 120−124.

(16) Clausen, H. F.; Chen, Y. S.; Jayatilaka, D.; Overgaard, J.; Koutsantonis, G. A.; Spackman, M. A.; Iversen, B. B. Intermolecular interactions and electrostatic properties of the β hydroquinone apohost: implications for supramolecular chemistry. *J. Phys. Chem. A* **2011**, *115*, 12962−12972.

(17) Steed, J. W.; Turner, D. R.; Wallace, K. J. *Core Concepts in Supramolecular Chemistry and Nanochemistry*; John Wiley & Sons: Chichester, England, 2007; pp 179−194.

(18) Atwood, J. L.; Davies, J. E. D.; MacNicol, D. D. *Inclusion Compounds*; Academic Press Inc.: London, 1984; Vol. 2.

(19) Powell, H. M. The Structure of Molecular Compounds. Part VIII. The Compounds of Krypton and Quinol. *J. Chem. Soc.* **1950**, 300−301.

(20) McAdie, H. G. Thermal Decomposition of Molecular Complexes: IV. Further Studies of the β Quinol Clathrates. *Can. J. Chem.* **1966**, *44*, 1373−1386.

(21) Palin, D. E.; Powell, H. M. The Structure of Molecular Compounds. Part VI. The β − Type Clathrate Compounds of Quinol. *J. Chem. Soc.* **1948**, *0*, 815−821.

(22) Torré, J. P.; Coupan, R.; Chabod, M.; Péré, E.; Labat, S.; Khoukh, A.; Brown, R.; Sotiropoulos, J. M.; Gornitzka, H. CO_2 − Hydroquinone Clathrate: Synthesis, Purification, Characterization and Crystal Structure. *Cryst. Growth Des.* **2016**, *16*, 5330−5338.

(23) Peyronel, G.; Barbieri, G. On Some New Clathrates of Hydroquinone. *J. Inorg. Nucl. Chem.* **1958**, *8*, 582−585.

(24) Palin, D. E.; Powell, H. M. The Structure of Molecular Compounds. Part III. Crystal Structure of Addition Complexes of Quinol with certain Volatile Compounds. *J. Chem. Soc.* **1947**, 208−221.

(25) Palin, D. E.; Powell, H. M. The Structure of Molecular Compounds. Part V. The Clathrate Compound of Quinol and Methanol. *J. Chem. Soc.* **1948**, 571−574.

(26) Wallwork, S. C.; Powell, H. M. The Structure of Molecular Compounds. Part XI. Crystal Structure of the Addition Complex of Quinol and Methyl Cyanide. *J. Chem. Soc.* **1956**, 4855−4858.

(27) Mak, C. W.; Lee, K. S. Hydroquinone Acetonitrile (3:1) clathrate. *Acta Crystallogr., Sect. B: Struct. Crystallogr. Cryst. Chem.* **1978**, *34*, 3631−3634.

(28) Lee, J. W.; Choi, K. J.; Lee, Y.; Yoon, J. H. Spectroscopic Identification and Conversion Rate of Gaseous Guest Loaded Hydroquinone Clathrates. *Chem. Phys. Lett.* **2012**, *528*, 34−38.

(29) Allison, S. A.; Barrer, R. M. Clathration by Phenol and Quinol. Part.II Kinetics. *Trans. Faraday Soc.* **1968**, *64*, 557−565.

(30) Jang, J. S.; Jeon, T. I.; Lee, Y. J.; Yoon, J. H.; Lee, Y. Characterization of α Hydroquinone and β Hydroquinone Clathrates by THz Time Domain Spectroscopy. *Chem. Phys. Lett.* **2009**, *468*, 37−41.

(31) Strobel, T. A.; Kim, Y.; Andrews, G. S.; Ferrell, J. R., III; Koh, C. A.; Herring, A. M.; Sloan, E. D. Chemical−Clathrate Hybrid Hydrogen Storage: Storage in Both Guest and Host. *J. Am. Chem. Soc.* **2008**, *130*, 14975−14977.

(32) Lee, J. W.; Yoon, J. H. Preferential Occupation of CO_2 Molecules in Hydroquinone Clathrates Formed from CO_2/N_2 Gas Mixtures. *J. Phys. Chem. C* **2011**, *115*, 22647−22651.

(33) Lee, J. W.; Dotel, P.; Park, J.; Yoon, J. H. Separation of CO_2 from Flue Gases using Hydroquinone Clathrate Compounds. *Korean J. Chem. Eng.* **2015**, *32*, 2507−2511.

(34) Lee, J. W.; Poudel, J.; Cha, M.; Yoon, S. J.; Yoon, J. H. Highly Selective CO_2 Extraction from a Mixture of CO_2 and H_2 Gases Using Hydroquinone Clathrates. *Energy Fuels* **2016**, *30*, 7604−7609.

(35) Lee, J. W.; Kang, S. P.; Yoon, J. H. Highly Selective Enclathration of Ethylene from Gas Mixtures. *J. Phys. Chem. C* **2014**, *118*, 6059−6063.

(36) Lee, J. W.; Kang, S. P.; Yoon, J. H. Competing Occupation of Guest Molecules in Hydroquinone Clathrates Formed from Binary C_2H_4 and CH_4 Gas Mixtures. *J. Phys. Chem. C* **2014**, *118*, 7705−7709.

(37) Coupan, R.; Plantier, F.; Torré, J. P.; Dicharry, C.; Sénéchal, P.; Guerton, F.; Moonen, P.; Khoukh, A.; Kessas, S. A.; Hemati, M. Creating Innovative Composite Materials to Enhance the Kinetics of CO_2 Capture by Hydroquinone Clathrates. *Chem. Eng. J.* **2017**, *325*, 35−48.

(38) Kohl, A.; Nielsen, R. *Gas Purification*; Gulf Publishing Co.: Houston, 1997.

(39) Coupan, R.; Péré, E.; Dicharry, C.; Torré, J. P. New Insights on Gas Hydroquinone Clathrates using in Situ Raman Spectroscopy: Formation/Dissociation Mechanisms, Kinetics and Capture Selectiv ity. *J. Phys. Chem. A* **2017**, *121*, 5450−5458.

(40) Kubinyi, M. J.; Keresztury, G. Infrared and Raman Spectra of Hydroquinone Crystalline Modifications. *Mikrochim. Acta* **1997**, *14*, 525−528.

(41) Jakobsen, R. J.; Brewer, E. J. Vibrational Spectra of Benzene Derivatives. I. Para Substituted Phenols. *Appl. Spectrosc.* **1962**, *16*, 32−35.

(42) Park, J. W.; An, S.; Seo, Y.; Kim, B. S.; Yoon, J. H. Temperature Dependent Release of Guest Molecules and Structural Transformation of Hydroquinone Clathrates. *J. Phys. Chem. C* **2013**, *117*, 7623−7627.

(43) Sandford, S. A.; Allamandola, L. J. The Physical and Infrared Spectral Properties of CO_2 in Astrophysical Ice Analogs. *Astrophys. J.* **1990**, *355*, 357−372.

(44) Wilmshurst, J. K.; Bernstein, H. J. The Infrared Spectra of CH_4, CH_3D, CH_2D_2, CD_3H and CD_4. *Can. J. Chem.* **1957**, *35*, 226−235.

(45) Coupan, R.; Chabod, M.; Dicharry, C.; Diaz, J.; Miqueu, C.; Torré, J. P. Experimental Determination of Phase Equilibria and Occupancies for CO_2, CH_4, and N_2 Hydroquinone Clathrates. *J. Chem. Eng. Data* **2016**, *61*, 2565−2572.

A Characterization Study of CO_2, CH_4, and CO_2/CH_4 Hydroquinone Clathrates Formed by Gas-Solid Reaction

Romuald COUPAN [1], Eve PÉRÉ [2], Christophe DICHARRY [1], Frédéric PLANTIER [3], Joseph DIAZ [1], Abdel KHOUKH [2], Joachim ALLOUCHE [2], Stephane LABAT [2], Virginie PELLERIN [2], Jean-Paul GRENET [2], Jean-Marc SOTIROPOULOS [2], Pascale SENECHAL [4], Fabrice GUERTON [4], Peter MOONEN [1,4], Jean-Philippe TORRE [1,]*

AUTHOR AFFILIATIONS.

1. CNRS/TOTAL/UNIV PAU & PAYS ADOUR, Laboratoire des Fluides Complexes et leurs Réservoirs-IPRA, UMR5150, Avenue de l'Université, 64000, PAU, France.

2. UNIV PAU & PAYS ADOUR, CNRS, Institut des Sciences Analytiques et de Physico-Chimie pour l'Environnement et les Matériaux (IPREM), UMR 5254, Hélioparc, Avenue du Président Pierre Angot, 64000, PAU, France.

3. CNRS/TOTAL/UNIV PAU & PAYS ADOUR, Laboratoire des Fluides Complexes et leurs Réservoirs-IPRA, UMR5150, Allée du Parc Montaury, 64600, ANGLET, France.

4. UNIV PAU & PAYS ADOUR, CNRS, DMEX-IPRA, UMS 3360, Avenue de l'Université, 64000, PAU, France.

Characterization apparatuses and methods.

The Raman spectroscopy analyses are performed using a T-64000 Jobin-Yvon spectrometer fitted with a Raman notch filter, a grating of 1,800 grooves/mm and a confocal microscope. The excitation source is the 514.5-nm line of an argon ion laser. Each analysis is conducted in the $3300 - 1100$ cm^{-1} region with an acquisition time of 60 seconds.

A customized Raman cell (from Top Industrie) is used to determine the structural transition (from β-HQ to α-HQ) temperature by tracking the spectral signature of the crystals as a function of temperature at the rate of 1 K/min, from ambient temperature to 393 K. This cell, equipped with a sapphire window of 35 mm in diameter, can be used to run in situ Raman spectroscopy experiments at pressures and temperatures of up to 20 MPa and 423 K respectively. At least six crystals are analyzed in each experiment to confirm repeatability and obtain averaged results. This paper does not give details on the apparatus used.[1]

Diffuse Reflectance Infrared Fourier Transform (DRIFT) spectroscopy measurements are performed using a Nexus Nicolet FT-IR spectrometer, purged with dried air, with a resolution of 4 cm^{-1}, after signal averaging 200 scans. Prior to sample analysis, the background spectrum is collected using pure KBr. The sample to be analyzed is ground and diluted to 10 wt% in powdered KBr. All spectra are recorded deducting the background contribution.

Cross-polarization/magic angle spinning (CP/MAS) solid-state ^{13}C NMR experiments, using a Bruker Avance 400 spectrometer, are conducted at ambient temperature with a resonance frequency of 100.61 MHz and a magic angle spinning rate of 7 kHz. The sample is placed in a zirconium rotor of 7 mm. The contact time and pulse delay are 3.8 ms and 5 s respectively. Chemical shifts are referenced to tetramethylsilane at 0 ppm, and a glycine carbonyl signal of 176 ppm serves as an external reference.

Clathrate morphology is evaluated by optical microscopy, scanning electron microscopy (SEM), transmission electron microscopy (TEM) and X-ray tomography. The TEM and SEM analyses were done at 293 K, and under vacuum (pressure close to 10^{-5} Pa). In these conditions, we did not observed any problems related to the HQ volatility during the analysis. Optical microscopy is performed by means of a camera (Qioptiq) with a zoom system of x16 which has a coaxial lighting LED system (from Edmund Optics) positioned beneath it. A Hirox-SH300 scanning electron microscope with an acceleration voltage of 20 kV is used for the SEM analyses. Each sample is placed on double-sided adhesive carbon tape and metalized with gold coating. The TEM images are taken with a Philips CM 200 (200 kV) with a LaB6 source. The samples, dispersed in CH_2Cl_2 (samples not soluble in this solvent), are dropped onto a carbon-coated copper grid and dried before analysis. X-ray tomography is performed using a Zeiss Xradia Versa 510T X-ray microscope (XRM). No specific sample preparation is required. Data are acquired using a tube voltage of 40 kV at 3 W. An exposure time of 35 s is selected. Each 3D dataset is obtained by reconstructing 2,001 independent radiographs. Data are analyzed with the help of Avizo 9 (FEI), Fiji [2] and Matlab (Mathworks).

Gas porosimetry experiments are achieved by N_2 adsorption–desorption at 77 K using the fully-automated Micromeritics TriStar II 3020 system, which makes it possible to obtain the textural parameters of micro- or mesoporous materials. The samples are purified at 308 K and 10 Pa for 24 hours before the measurements are performed.

Thermogravimetric analyses (TGA), using a SETSYS Evolution 1750 CS TG analyzer, are performed under helium flow at 20 cm^3/min. A heating ramp of 5 K/min from ambient temperature to 573 K is applied to the sample in the crucible. The sample mass is tracked as a function of time. Gas released during the thermal decomposition is immediately analyzed by a coupled mass spectrometer – OmniStar GSD 301 02.

By measuring the sample mass before and after the enclathration reaction it is possible to evaluate mass balances and deduce the total amount of gas captured by the HQ. These measurements are performed using an analytical balance with an uncertainty of ± 0.001 g.

(1) Coupan, R.; Péré, E.; Dicharry, C.; Torré, J.-P. New Insights on Gas Hydroquinone Clathrates using in Situ Raman Spectroscopy: Formation/Dissociation Mechanisms, Kinetics and Capture Selectivity. *J. Phys. Chem. A* **2017**, *121*, 5450-5458.

(2) Schindelin, J.; Arganda-Carreras, I.; Frise, E.; Kaynig, V.; Longair, M.; Pietzsch, T.; Preibisch, S.; Rueden, C.; Saalfeld, S.; Schmid B. et al. Fiji: an Open-Source Platform for Biological-Image Analysis. *Nat Methods* **2012**, *9*, 676-682.
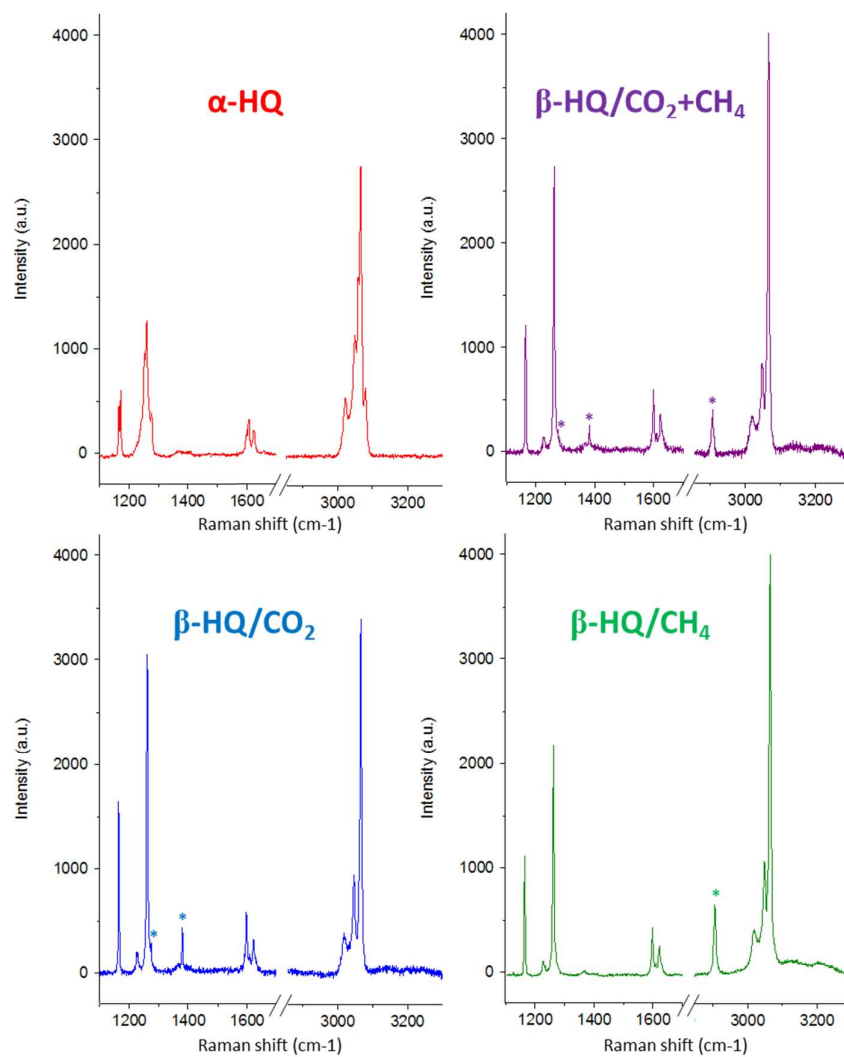
Spectroscopic identification.

Figure S1. Raman spectra ranging from 1100 to 3300 cm^{-1}: (red) α-HQ and (blue) CO$_2$-, (purple) CO$_2$/CH$_4$- and (green) CH$_4$-HQ clathrates. The asterisks * show the Raman bands observed for CO$_2$ and CH$_4$ molecules.
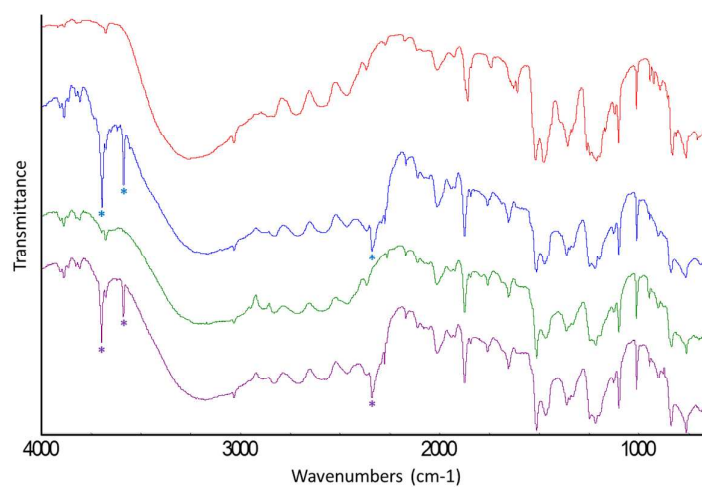
Figure S2. IR spectra: (red) α-HQ and (blue) CO_2, (purple) CO_2/CH_4 and (green) CH_4 HQ

clathrates. The asterisks * show the IR bands observed for CO_2 molecules.

Gas storage capacity.

Table S1. Gas storage capacities (mol^{Guest}/kg^{HQ}) of CO_2-, CO_2/CH_4- and CH_4-HQ clathrates obtained after 1 month's reaction at 3.0 MPa and at ambient temperature.

	CH₄	*CO₂/CH₄*	*CO₂*
TGA	0.73 ± 0.16	2.17 ± 0.15	2.87 ± 0.14
Mass balance	0.69 ± 0.34	2.36 ± 0.14	2.85 ± 0.04
Average	*0.71 ± 0.36*	*2.26 ± 0.24*	*2.86 ± 0.14*